Atmos. Meas. Tech. Discuss., 7, 4693–4727, 2014
www.atmos-meas-tech-discuss.net/7/4693/2014/
doi:10.5194/amtd-7-4693-2014

Atmospheric Measurement Techniques Discussions

Characteristics of tropopause parameters as observed with GPS radio occultation

T. Rieckh[1,2], B. Scherllin-Pirscher[1,2], F. Ladstädter[1,2], and U. Foelsche[2,1]

[1]Wegener Center for Climate and Global Change, University of Graz, Graz, Austria
[2]Institute for Geophysics, Astrophysics, and Meteorology/Institute of Physics (IGAM/IP), University of Graz, Graz, Austria

Received: 15 April 2014 – Accepted: 16 April 2014 – Published: 8 May 2014

Correspondence to: T. Rieckh (therese.rieckh@uni-graz.at)

Published by Copernicus Publications on behalf of the European Geosciences Union.

Abstract

Characteristics of the lapse rate tropopause are analyzed globally for tropopause altitude and temperature using Global Positioning System (GPS) Radio Occultation (RO) data from late 2001 to 2012. RO profiles feature high vertical resolution and excellent quality in the upper troposphere and lower stratosphere, which are key factors for tropopause determination, including multiple ones. Furthermore, global coverage is reached on a monthly basis, allowing to examine both temporal and spatial characteristics thoroughly. To investigate latitudinal and longitudinal tropopause characteristics, the mean annual cycle, and inter-annual variability, we use tropopauses from individual profiles as well as their monthly mean and median for 10° zonal bands. The latitudinal structure of first tropopauses shows the well-known distribution with high (cold) tropical tropopauses and low (warm) extratropical tropopauses. In the transition zones (20° N/S to 40° N/S), individual profiles reveal varying tropopause altitudes from 7 km to 17 km due to the influence of the subtropical jets. In this region, we also find multiple tropopauses throughout the year. Longitudinal variability is strongest at northern hemispheric mid latitudes and in the Asian monsoon region. The mean annual cycle features changes in amplitude and phase depending on latitude. This is caused by different underlying physical processes (such as the Brewer-Dobson Circulation) and atmospheric dynamics (such as the very strong polar vortex in southern hemispheric winter). Inter-annual anomalies of tropopause parameters show signatures of El Niño–Southern Oscillation, the Quasi-Biennial Oscillation, and the varying strength of the polar vortex, including sudden stratospheric warming events.

1 Introduction

The tropopause marks the transition between the well-mixed troposphere and the stably stratified stratosphere. Besides the change in stratification, fundamental changes in the composition of chemical constituents such as water vapor or ozone take place in

AMTD
7, 4693–4727, 2014

this region (Holton et al., 1995). The tropopause generally acts as a dynamic barrier for cross-tropopause transport. Exchange between troposphere and stratosphere is characterized by deep convection in the tropics, which is the main source for water vapor in the stratosphere and plays an important role in stratospheric chemistry (Fueglistaler et al., 2009). In the extratropics, stratosphere-troposphere exchange takes place via quasi-horizontal transport at the edge of subtropical and polar jets, affecting tropospheric ozone concentrations and hence tropospheric and surface climate (Gettelman et al., 2011).

Tropopause properties do not only contain information about possible troposphere-stratosphere exchange, but can also be associated with the state of certain atmospheric characteristics. For example, due to their simple latitudinal structure, tropopause pressure or tropopause altitude characteristics can serve as a measure for the width of the tropical belt (Seidel and Randel, 2007; Birner, 2010).

Tropopause characteristics react to both tropospheric and stratospheric temperature changes. Studies about tropopause altitude changes as an indicator of climate change have been conducted, e.g., by Santer et al. (2003), Sausen and Santer (2003), and Seidel and Randel (2006). All these studies consistently found evidence of a decrease in global tropopause temperature and pressure (increase in tropopause altitude) due to anthropogenic tropospheric warming and lower stratospheric cooling (e.g., Santer et al., 2004).

During the last decades, radiosonde data have been the most important data source to study tropopause parameters and their characteristics (e.g., Randel et al., 2000; Seidel et al., 2001). With their multiple-decade long data record and high vertical resolution, these measurements are very valuable for monitoring inter-annual and intra-annual variations of tropopause parameters. On the other hand, coverage in the Southern Hemisphere (SH) and above oceans is very poor, which makes it hard to catch spatial characteristics and changes. Thus analysis and reanalysis products have been used alternatively to investigate tropopause characteristics globally (see, e.g., Hoinka, 1998; Highwood and Hoskins, 1998).

AMTD
7, 4693–4727, 2014

However, to investigate tropopause properties fully based on observational data, the relatively new Global Positioning System (GPS) Radio Occultation (RO) technique has been increasingly used during the last years. The RO method (Melbourne et al., 1994; Kursinski et al., 1997; Hajj et al., 2002; Kuo et al., 2004) provides near-vertical profiles of atmospheric thermodynamic variables with high vertical resolution (better than 1 km) and global coverage. Other features of RO measurements include all-weather capability, high accuracy, high precision, and long-term stability (see, e.g., Anthes, 2011). A number of studies confirmed the feasibility and excellent eligibility of RO measurements for monitoring the atmosphere (Foelsche et al., 2008, 2009) and for climate change detection (Leroy et al., 2006; Schmidt et al., 2008; Steiner et al., 2011).

The combination of the excellent RO profile quality in the upper troposphere and lower stratosphere (Kursinski et al., 1997) and data availability above ocean and land (including polar regions) makes these data highly suited for tropopause parameter evaluation. First studies using GPS RO data for tropopause determination have been conducted by Schmidt et al. (2004, 2005) for both the tropical region and globally. As RO data proved to provide accurate information on tropopause characteristics, these data have been increasingly used during the last years (see, e.g., Kishore et al., 2006; Borsche et al., 2007; Foelsche et al., 2009; Son et al., 2011). Recently, a new method for tropopause determination from RO profiles based on bending angle information has been introduced by Lewis (2009). This technique can be applied earlier in the RO data retrieval, avoiding additional processing. Schmidt et al. (2010) compared tropopause data resulting from this algorithm to conventional lapse rate tropopause data and found generally good agreement.

So far tropopause characteristics have mainly been analyzed based on spatio-temporal means. This implies that information about the distribution of individual tropopause features gets lost. The aim of this paper is to use single RO profiles to investigate tropopause altitude (H_T) and temperature (T_T) on a global scale. Differences in mean and median will give insight to the distribution within 10° latitudinal

AMTD
7, 4693–4727, 2014

bands. Furthermore, the dense field of RO profiles (available since 2006) will be used to analyze small-scale spatio-temporal characteristics.

The structure of this paper is as follows: in Sect. 2, descriptions of the RO measurement principle, the tropopause algorithm, and the binning method are given. In Sect. 3, latitudinal and longitudinal characteristics are discussed. Section 4 describes the annual cycle of averaged tropopause data for different latitudinal bands and in Sect. 5, inter-annual variability is discussed. Section 6 provides a summary.

2 Data and methods

2.1 RO measurement principle

The GPS RO method is a limb sounding technique and uses electromagnetic signals transmitted by GPS satellites, which are received by a Low Earth Orbit (LEO) satellite. The GPS signals are delayed and refracted by the Earth's atmosphere. The measured quantity onboard the LEO satellite is the phase change as a function of time between the intrinsically transmitted signal and the received frequency-shifted signal. Due to the satellites' motion, the atmosphere is scanned, which yields a profile of phase changes. By including precise orbit information it can be transformed into a bending angle profile. Using an Abel transform, bending angle profiles are processed to refractivity profiles.

To first order, refractivity depends on dry air density and humidity, as described by the Smith-Weintraub formula (Smith and Weintraub, 1953). In the so-called dry air retrieval, presence of water vapor is attributed to the dry atmospheric parameters. Applying the Smith-Weintraub formula, hydrostatic equation, and the equation of state yields dry density, dry temperature, and dry pressure. For the detailed retrieval description, see Kursinski et al. (1997). Physical atmospheric parameters can be derived by including background information and applying a 1D-Var retrieval (Healy and Eyre, 2000).

For tropopause computation, we use atmospheric profiles retrieved with the WEGC (Wegener Center for Climate and Global Change) Occultation Processing System

AMTD
7, 4693–4727, 2014

(OPS) Version 5.6 (Schwärz et al., 2013) from the following satellite missions: CHAMP (CHAllenging Mini-Satellite Payload): September 2001 to September 2008; F3C (Formosa Satellite Mission 3/Constellation Observing System for Meteorology, Ionosphere, and Climate): April 2006 to December 2012; GRACE-A (Gravity Recovery And Climate Experiment): March 2007 to December 2012. During the CHAMP period, approximately 5000 profiles per month were available globally. The number of measurements strongly increased with the launch of the six F3C satellites to approximately 60 000 profiles per month. The investigated time range covers September 2001 through December 2012.

2.2 Tropopause algorithm

There exist several tropopause definitions, such as the chemical, dynamical, or the thermal definition. The lapse rate definition has the advantage that it is easy to apply and commonly used, which allows the comparison to other studies. We therefore apply the lapse rate tropopause definition of the World Meteorological Organization (WMO) to individual RO temperature profiles and compute tropopause altitude H_T and temperature T_T. According to the WMO (1957), the tropopause is defined as the lowest level at which the lapse rate decreases to $2\,^{\circ}\mathrm{C\,km^{-1}}$ or less, provided that the average lapse rate from this point to any other point within the next two kilometers does not exceed $2\,^{\circ}\mathrm{C\,km^{-1}}$ either. This ensures not to accidentally take a shallow stable layer in the troposphere for the tropopause (Homeyer et al., 2010). For the profile shown in Fig. 1, this criterion is fulfilled at 13.5 km.

For multiple tropopauses, the WMO (1957) states that if at any point above the first tropopause the average lapse rate between this point and any point within the next higher kilometer exceeds $3\,^{\circ}\mathrm{C\,km^{-1}}$, an additional tropopause may be found, using the same criterion as before. In Fig. 1, the lapse rate exceeds $3\,^{\circ}\mathrm{C\,km^{-1}}$ between 15 km and 17 km. At 17.3 km, a second lapse rate tropopause is found. The local minimum of the temperature profile, i.e. the cold point tropopause, is located slightly higher at

AMTD
7, 4693–4727, 2014

17.5 km. T_T is computed directly from the temperature profile by choosing the value according to H_T.

We apply the tropopause algorithm to dry temperature profiles as differences between dry and physical temperatures become negligible at tropopause altitudes for most latitudes (Scherllin-Pirscher et al., 2011; Danzer et al., 2014).

However, high concentrations of water vapor in the lower troposphere can lead to temperature gradients, which may be interpreted as tropopauses by the algorithm. In order to exclude these "tropopauses", we apply the algorithm only above a certain altitude, which depends on latitude and season (approximately 6 km in the extratropics and 12 km in the tropics). Furthermore, we restrict the algorithm to a top altitude of 22 km and search for three tropopauses at most. Figure 2 exemplarily shows dry temperature profiles and their tropopauses for January 2004 with all constraints described above.

2.3 Averaging method

In this work, the main focus lies on tropopause characteristics derived from individual profiles. In addition, averaged data are used to investigate latitudinal characteristics in more detail. We therefore calculate the latitude-weighted mean (H_{mean}, T_{mean}) and the median (H_{med}, T_{med}) for 10° latitudinal bands on a monthly basis. Differences in mean and median allow to conclude on how tropopause parameters are distributed within the 10° latitudinal bands.

3 Spatial characteristics

3.1 Latitudinal characteristics

Figure 3 shows the latitudinal distribution of H_T for January and July 2008. H_{mean} and H_{med} for 10° latitudinal bands are additionally shown in Fig. 3 and listed in Table 1.

AMTD
7, 4693–4727, 2014

Concerning latitudinal variations of the first tropopause, two well-defined regions can be distinguished. While tropical tropopauses are found at 15 km to 18 km, extratropical tropopauses occur at lower altitudes between 6 km and 12 km. This pattern results from the dominant physical processes, which are different for the tropics and extratropics. While high tropical H_T occur due to radiative-convective balance, lower extratropical H_T are caused by baroclinic wave dynamics (Gettelman et al., 2011).

In the summer hemisphere, the transition from tropical to extratropical H_T is rather smooth. In the winter hemisphere, the situation is fundamentally different. Rather than a steady decrease of H_T with latitude, there is a jump from tropical to extratropical characteristics within the 20° N/S to 30° N/S latitudinal band. This leads to a large spread of H_T from 7 km to 17 km. The seasonal differences can also be seen in H_{mean} and H_{med} (see Fig. 3 and Table 1).

Comparing H_{mean} and H_{med} generally shows good agreement for all latitudes and seasons, with differences smaller than 500 m. Larger deviations are found between 20° and 30° in hemispheric winter, when the strong subtropical jet leads to large variations in the H_T distribution. The higher H_{med} compared to H_{mean} indicates that the major part of tropopauses is located at high altitudes, but the few tropopauses with extratropical characteristics lower H_{mean} significantly.

Differences between H_{mean} and H_{med} can also be found at SH high latitudes in winter. Extremely high H_T, as found between 12 km and 18 km, raise the mean, and differences between H_{mean} and H_{med} exceed 1 km. These high H_T may result from a deficiency of the lapse rate tropopause definition, because it is not well suited for very cold stratospheric conditions as found in SH polar winter (Zängl and Hoinka, 2001).

The sharp, stepwise edges of lowermost occurring tropopauses in the subtropics and mid latitudes in Fig. 3 are due to a combination of the bottom search altitude as defined in the tropopause algorithm (see Sect. 2.2) and dry temperature variations caused by changing water vapor concentrations. These variations may be occasionally identified as tropopauses by the algorithm.

AMTD
7, 4693–4727, 2014

Figure 3 also shows the latitudinal distribution of second and third tropopauses. Multiple tropopauses mainly occur at subtropical latitudes throughout the year and at mid and high latitudes in winter. Fewer multiple tropopauses can be found in the tropics.

Multiple tropopauses close to the subtropical jet are associated with latitudinal migration of the tropical over the subtropical tropopause (Randel et al., 2007). Multiple tropopause occurrence is more frequent during hemispheric winter when the jet is stronger.

In the winter hemisphere, multiple tropopause occurrence also expands further polewards, reflecting the unstable stratospheric conditions with low stratification, and H_T of second tropopauses spread between 13 km and 22 km.

Double tropopauses in the tropics can be found throughout the year and are likely caused by planetary scale waves. Equatorial Kelvin waves with strong amplitudes can modify the temperature profile and thus its lapse rate, which can lead to double tropopauses (Randel et al., 2007).

Mean and median of second tropopauses are generally in good agreement as differences rarely exceed 200 m. In the extratropics, mean and median are located approximately at mean tropical first tropopause altitudes. In the tropics, they are up to 2.5 km higher.

In Fig. 4, tropopause temperature T_T for January and July 2008 is shown as a function of latitude. The distribution of T_T is much smoother than that of H_T. Generally, tropopause temperature inversely correlates with tropopause altitude.

High tropical tropopauses feature low temperatures with T_T ranging from 180 K to 200 K. Lower and therefore warmer extratropical tropopauses reach temperatures of up to 230 K. Due to the extremely cold polar vortex in SH winter, T_T drops to very low values at SH high latitudes.

As for H_T, larger differences between T_{mean} and T_{med} are found for the 20° to 30° latitudinal band in hemispheric winter. T_{mean} is up to 4 K higher than T_{med} (see Table 2). However, the differences seen in H_{mean} and H_{med} in SH polar winter are not

AMTD
7, 4693–4727, 2014

found in T_{mean} and T_{med} because of the cold and stably stratified, nearly isothermal, stratosphere.

For the second tropopause, Fig. 4 shows 5 K to 10 K higher monthly averaged tropopause temperatures in the tropics and summer hemispheric high latitudes than for the first tropopause. In winter hemispheric high latitudes, average tropopause temperatures are lower for the second than for the first tropopause. This difference can exceed 10 K (see Table 2).

3.2 Longitudinal characteristics

Longitudinal variations in H_T and T_T occur due to land and sea coverage and orography. Figures 5 and 6 show H_T and T_T of individual RO measurements for January, April, July, and October 2008. It is obvious that longitudinal variations of tropopause parameters are much smaller than latitudinal variations.

Zonal asymmetries appear especially at Northern Hemispheric (NH) mid latitudes (40° N to 60° N). These asymmetries are strongest in NH winter, but can still be found in spring and fall. For January, Fig. 5 shows exceptionally low H_T above eastern Canada as well as above eastern Russia and the western part of the North Pacific. This pattern occurs due to large-scale Rossby wave troughs at the eastern side of continents (Zängl and Hoinka, 2001). H_T varies between less than 8 km and 10 km in these areas, while H_T is at 10 km to 13 km above the eastern North Pacific and the North Atlantic. The pattern becomes weaker in NH spring. During NH summer, these zonal asymmetries vanish as Rossby wave activity is weakest during that time of the year.

Figure 5 also shows zonal asymmetries in the tropics/subtropics in NH summer (July). While H_{mean} and H_{med} are close to 16 km for the 20° N to 40° N latitudinal bands (see Table 1), H_T reaches more than 17 km above South Asia. This pattern is caused by deep convective activity in the Asian monsoon region (Highwood and Hoskins, 1998).

In the SH, zonal asymmetries are generally less pronounced than in the NH due to fewer orographic influences. Tropopause patterns resulting from Rossby wave activity can still be found at SH mid latitudes (40° S to 60° S).

AMTD
7, 4693–4727, 2014

T_T (Fig. 6) generally shows zonal patterns similar to H_T. The asymmetry in NH winter at NH mid latitudes is also strong here, with high T_T of 218 K to more than 225 K above the western part of the North Pacific and eastern Canada. Above most of Europe and Asia, T_T is 10 K to 15 K lower. In July, the very high H_T above South Asia again corresponds to low T_T. Furthermore, exceptionally low T_T are found over the Maritime Continent.

4 The annual cycle

To investigate the mean annual cycle at different latitudes, we average over H_{mean} and H_{med} (T_{mean} and T_{med}) for every month. Figure 7 shows the mean annual cycle for mean and median of H_T and T_T for 10° latitudinal bands.

Generally, H_T follows the cycle of incoming radiation, with maximum altitudes in summer, a decrease in fall, minimum altitudes in winter, and an increase in spring.

The mean annual cycle is very pronounced in the subtropics and mid latitudes, with amplitudes of more than 2 km. The amplitude decreases towards tropics and high latitudes.

In the tropics, the annual cycle is weak as H_T changes are only about 1 km. In the NH tropics, between the equator and 20° N, H_T shows an annual cycle with maximum altitudes in winter and minimum altitudes in summer due to the strong influence of the Brewer-Dobson Circulation (BDC) on H_T. The BDC NH branch has a strong annual cycle, with maximum tropical upwelling in winter (Yulaeva et al., 1994). As a result, tropical tropopause altitudes are highest in winter.

At high latitudes, the mean annual cycle of H_T behaves fundamentally different for NH and SH. In the NH, the annual cycle is a combination of two waves. These are a single wave pattern over subpolar eastern Siberia and North America with maximum H_T in NH summer (minimum H_T in NH winter), and a double wave pattern over northern Europe, western Siberia, and high Arctic latitudes with maximum H_T in NH summer and NH winter (minimum H_T in NH spring and NH fall) (Zängl and Hoinka, 2001). In

AMTD
7, 4693–4727, 2014

the SH, a reversed mean annual cycle occurs over Antarctica. It can be explained by the gradual decrease of stratospheric temperatures during SH winter due to the lack of incoming radiation. Minimum stratospheric temperatures and thus highest H_T are observed in August. Due to the shift in phase from mid latitudes to high latitudes, there is no pronounced cycle at all for the latitudinal band 50° S to 60° S.

The comparison of mean and median shows good agreements except for the latitudinal bands 20° N/S to 30° N/S. Differences between mean and median in this region have already been found for January and July as shown in Fig. 3 and Table 1. However, the complete annual cycle gives further insight in the development of tropopause distribution. In the NH, the median has a very weak annual cycle, that follows the one of the tropical tropopauses. Due to strong equatorial upwelling in NH winter, most tropopauses are pushed to high altitudes even within the 20° N to 30° N latitudinal band. The mean, on the other hand, is strongly affected by the very low tropopauses occurring in this region (see Fig. 3). In NH summer, such very low tropopauses do not occur due to the smooth decrease of H_T from low to high latitudes. Therefore the mean has a pronounced annual cycle, following the one of mid latitudes. As a result, mean and median agree very well during NH summer, but differences between mean and median increase in NH fall and maximize (1 km) in NH winter.

In the SH, the situation is different as the annual cycle of H_T has the same phase in the tropics and subtropics. The median is always higher than the mean as more tropopauses show tropical characteristics. The resulting offset is 0.5 km in SH summer and 1 km in SH winter.

The shift from tropical to extratropical tropopause characteristics also causes minor differences between mean and median at latitudes from 30° N/S to 50° N/S.

The mean annual cycle of T_T is shown in Fig. 7 (right panel). Again, high H_T correspond to low T_T and vice versa. A weak annual cycle is found in the tropics with amplitudes of less than 3 K. It increases towards mid latitudes to about 5 K.

In the NH, there is hardly any annual cycle for the 40° to 50° latitudinal band, and a shift in phase towards high latitudes. Similar to Zängl and Hoinka (2001), we also

AMTD
7, 4693–4727, 2014

find a single wave pattern of T_T with maximum temperatures in polar NH summer and minimum temperatures in NH winter, rather than a mixed wave pattern as found for H_T. The amplitude of this T_T annual cycle ranges from 2.5 K to 5 K, increasing towards higher latitudes.

In the SH, the annual cycle of T_T inversely follows the one of H_T for all latitudes, including the six-month shift of its phase from approximately 50° S polewards. In this region, the amplitude strongly increases with latitude to more than 12 K at polar latitudes. T_T is much lower in SH winter than NH winter. This difference is caused by the extremely cold polar vortex in the SH on the one hand, and the more frequent occurrence of Sudden Stratospheric Warming (SSW) events in the NH on the other hand. During SSW events, stratospheric temperatures can increase by up to 50 K within a couple of days, which affects T_T.

Differences in mean and median of T_T correspond to differences in mean and median of H_T.

5 Inter-annual variability

As the tropopause is influenced by both tropospheric and stratospheric conditions, anomalies in tropopause properties can be caused by events in the troposphere, such as El Niño–Southern Oscillation (ENSO) cold and warm phases, or in the stratosphere, such as SSW events or the Quasi-Biennial Oscillation (QBO).

ENSO has an impact on weather and climate on a global scale (Free and Seidel, 2009). ENSO warm phases cause tropospheric warming and stratospheric cooling (Lau et al., 1998). For zonal mean temperatures at low and mid latitudes, the ENSO signal shows a transition from warming to cooling near the tropopause. However, the transition of the local temperature response occurs well below the tropopause (Scherllin-Pirscher et al., 2012), yielding strong longitudinal variations of tropopause characteristics (Gage and Reid, 1987).

AMTD
7, 4693–4727, 2014

Therefore H_T and T_T from individual profiles are used in the following. Figures 8 and 9 show tropopause altitude and temperature for a cold ENSO phase (top panels, January 2008) and a warm ENSO phase (bottom panels, January 2010). Since we focus on the region between 40° S and 40° N, the colorbars are restricted to 15.5 km to 17.5 km and 185 K to 205 K, respectively.

Generally, the temperature pattern is much smoother than the altitude pattern. Strongest ENSO signals occur above the tropical central Pacific (100° W to 160° W) and the Maritime Continent (100° E to 160° E). During the ENSO cold phase, an area with decreased H_T (increased T_T) occurs above the tropical central Pacific. Above the western Pacific and Indonesia, H_T is significantly higher (T_T is lower). During the ENSO warm phase, these patterns are reversed for both tropopause altitude and temperature. These results are consistent with Randel et al. (2000).

To investigate the zonal mean response of tropopause parameters to inter-annual atmospheric variability, anomalies are computed by subtracting the annual cycle from H_{mean} and H_{med} (T_{mean} and T_{med}). Anomalies of H_{mean}, H_{med} (red, orange) and T_{mean}, T_{med} (dark blue, light blue) for the different latitudinal bands are shown in Fig. 10 (NH) and Fig. 11 (SH).

In the tropics, variations are generally small with altitude (temperature) anomalies being smaller than 750 m (3 K) between September 2001 and December 2012. These variations are caused by a combination of QBO and ENSO (Randel et al., 2000). Within our time range, correlation of H_T (T_T) anomalies and QBO (Singapore winds at 50 hPa) maximizes at the equator with values of around 0.5 for a lag of zero/one months (not shown). ENSO correlation for H_T shows off-equatorial maxima at 10° to 20° of 0.6 for a lag of two/three months. For T_T, the correlation is slightly smaller.

Anomalies at latitudes between 20° and 50° show some variability, but no distinct pattern. However, at high latitudes, stratospheric conditions have a strong impact on polar H_T and T_T, especially in winter and spring.

AMTD
7, 4693–4727, 2014

SSW events have a strong influence on tropopause characteristics. During SSW events, stratospheric temperatures increase by up to 50 K within a couple of days (Kuttippurath and Nikulin, 2012) and cause low H_T and high T_T.

In the NH, relatively strong SSW events occurred in winter 2003/2004, 2005/2006, 2008/2009, and 2009/2010 during the observed time range. Figure 10 shows lower H_T and higher T_T for these months. In January/February 2005, 2007, and 2011, when no or only a very weak SSW event occurred, tropopause anomalies are significantly higher and colder (up to 1.5 km/7 K) at NH high latitudes. Generally, the signal appears not only at polar latitudes, but between 60° N and 90° N.

During the observed time range, only one SSW event took place in the SH. In Fig. 11, H_T anomalies of −2 km (T_T anomalies of 10 K) can be seen for late 2002 for the 80° S to 90° S latitudinal band. This event was so strong that it even affected tropopause characteristics in the 50° S to 60° S latitudinal band. Stratospheric conditions were also exceptionally warm for winter and spring 2004 over the Antarctic region (NOAA, 2010), yielding tropopause altitude and temperature anomalies of −1 km and 3 K. For the years 2006, 2008, 2010, and 2011 the polar vortex was very cold and stable often lasting until December (see, e.g., NOAA, 2010). This led to unusually cold stratospheric conditions and as a consequence to high H_T and low T_T.

6 Summary

In this study, Radio Occultation (RO) data were used to investigate characteristics of the global lapse rate tropopause. We used data from September 2001 to December 2012, which cover almost the full RO observational record. Latitudinal and longitudinal variations as well as the annual cycle and inter-annual variability were analyzed for the tropopause parameters altitude (H_T) and temperature (T_T).

Tropopause properties were analyzed using individual measurements as well as averaged data. Both mean (H_{mean}, T_{mean}) and median (H_{med}, T_{med}) were computed to obtain information about the distribution of H_T and T_T within 10° latitudinal bands.

AMTD
7, 4693–4727, 2014

H_T and T_T showed the well-known latitudinal structure with high and cold tropical tropopauses (15 km to 18 km/180 K to 200 K) and lower and warmer extratropical tropopauses (6 km to 12 km/up to 230 K). Multiple tropopauses were found at the equator, close to the subtropical jets, and at winter hemispheric mid and high latitudes.

The strong subtropical jet leads to a large spread in the H_T and T_T distribution in the 20° to 30° latitudinal band during winter. Since the major part of tropopauses is located at high altitudes, but some tropopauses also show extratropical characteristics, H_{med} is systematically higher than H_{mean}. Differences can exceed 1.5 km in the Northern Hemisphere (NH) and 1 km in the Southern Hemisphere (SH). Accordingly, T_{mean} is up to 4 K higher than T_{med}. For second tropopauses, mean and median of H_T and T_T generally show small differences and are located approximately at tropical tropopause altitudes/temperatures.

Longitudinal variations of H_T and T_T occur due to land/sea coverage and orography. Zonal asymmetries at NH mid latitudes (40° to 60°) are caused by large-scale Rossby wave activity, most pronounced in NH winter (Zängl and Hoinka, 2001). In NH summer, strong convective activity in the Asian monsoon region leads to exceptionally high and cold tropopauses (Highwood and Hoskins, 1998).

The mean annual cycles of H_T and T_T vary strongly in amplitude with latitude. While smallest amplitudes were found in the tropics, amplitudes were largest at mid and SH high latitudes. At NH low latitudes, tropopause parameters follow the annual cycle of the Brewer-Dobson Circulation (BDC) with maximum tropical upwelling in winter, leading to higher/colder tropopauses in winter than in summer. Therefore the mean annual cycle is in phase within 20° S and 20° N. A six months phase shift of the annual cycle was found over Antarctica. Due to the lack of incoming radiation in SH polar winter and the strong polar vortex, very low stratospheric temperatures lead to highest H_T (lowest T_T) during that time of the year.

The mean annual cycle of H_{mean} and H_{med} (T_{mean} and T_{med}) agreed well for all latitudinal bands except 20° N/S to 30° N/S. In this region, the mean was systematically lower than the median throughout the year. Furthermore, the 20° N to 30° N median followed

AMTD
7, 4693–4727, 2014

the tropical tropopause annual cycle as most tropopauses are located at high altitudes. The mean, however, is affected by some very low tropopauses that mainly occur during NH winter and therefore followed the extratropical tropopause annual cycle.

Concerning inter-annual variability, we found patterns in tropopause anomalies caused by El Niño–Southern Oscillation (ENSO), Quasi-Biennial Oscillation (QBO), and Sudden Stratospheric Warming (SSW) events. The ENSO signal was strongest in the tropical central Pacific and Maritime Continent. During an ENSO cold phase, H_T was higher (T_T was lower) above the Maritime Continent and H_T was lower (T_T was higher) above the tropical central Pacific. This pattern reversed for the ENSO warm phase.

Anomalies of H_{mean}, H_{med}, T_{mean}, and T_{med} showed signatures of both ENSO and QBO at low latitudes. At high latitudes, large anomalies could be attributed to strong variability of polar vortex strength, including SSW events.

The ability to detect reliable trends in the relatively short RO record is limited by the large atmospheric variability during the last couple of years (e.g., strong El Niño event in 2009/2010 and two strong La Niña events in 2010/2011 and 2011/2012). Even for multiple linear regression analysis (including ENSO and QBO), tropopause trends were inconclusive for different periods (2001–2010; 2001–2012). Therefore we did not include a discussion of tropopause parameter trends in this paper.

Acknowledgements. We would like to acknowledge UCAR/CDAAC for the provision of level 1 RO data and WEGC for the provision of level 2 RO data. Special thanks to M. Schwärz and J. Fritzer for the contributions in OPS system development and operations. This study was funded by the Austrian Science Fund (FWF) under research grants P22293-N21 (BENCHCLIM) and T620-N29 (DYNOCC).

AMTD
7, 4693–4727, 2014

References

Anthes, R. A.: Exploring Earth's atmosphere with radio occultation: contributions to weather, climate and space weather, Atmos. Meas. Tech., 4, 1077–1103, doi:10.5194/amt-4-1077-2011, 2011. 4696

Birner, T.: Recent widening of the tropical belt from global tropopause statistics: sensitivities, J. Geophys. Res., 115, D23109, doi:10.1029/2010JD014664, 2010. 4695

Borsche, M., Kirchengast, G., and Foelsche, U.: Tropical tropopause climatology as observed with radio occultation measurements from CHAMP compared to ECMWF and NCEP analyses, Geophys. Res. Lett., 34, L03702, doi:10.1029/2006GL027918, 2007. 4696

Danzer, J., Foelsche, U., Scherllin-Pirscher, B., and Schwärz, M.: Influence of changes in humidity on dry temperature in GPS RO climatologies, Atmos. Meas. Tech. Discuss., submitted, 2014. 4699

Foelsche, U., Borsche, M., Steiner, A. K., Gobiet, A., Pirscher, B., Kirchengast, G., Wickert, J., and Schmidt, T.: Observing upper troposphere–lower stratosphere climate with radio occultation data from the CHAMP satellite, Clim. Dynam., 31, 49–65, doi:10.1007/s00382-007-0337-7, 2008. 4696

Foelsche, U., Pirscher, B., Borsche, M., Kirchengast, G., and Wickert, J.: Assessing the climate monitoring utility of radio occultation data: from CHAMP to FORMOSAT-3/COSMIC, Terr. Atmos. Ocean. Sci., 20, 155–170, doi:10.3319/TAO.2008.01.14.01(F3C), 2009. 4696

Free, M. and Seidel, D. J.: Observed El Niño–Southern Oscillation temperature signal in the stratosphere, J. Geophys. Res., 114, D23108, doi:10.1029/2009JD012420, 2009. 4705

Fueglistaler, S., Dessler, A. E., Dunkerton, T. J., Folkins, I., Fu, Q., and Mote, P. W.: Tropical tropopause layer, Rev. Geophys., 47, RG1004, doi:10.1029/2008RG000267, 2009. 4695

Gage, K. S. and Reid, G. C.: Longitudinal variations in tropical tropopause properties in relation to tropical convection and ENSO events, J. Geophys. Res., 92, 14197–14203, 1987. 4705

Gettelman, A., Hoor, P., Pan, L. L., Randel, W. J., Hegglin, M. I., and Birner, T.: The extratropical upper troposphere and lower stratosphere, Rev. Geophys., 49, RG3003, doi:10.1029/2011RG000355, 2011. 4695, 4700

Hajj, G. A., Kursinski, E. R., Romans, L. J., Bertiger, W. I., and Leroy, S. S.: A technical description of atmospheric sounding by GPS occultation, J. Atmos. Sol.-Terr. Phy., 64, 451–469, doi:10.1016/S1364-6826(01)00114-6, 2002. 4696

AMTD
7, 4693–4727, 2014

Healy, S. B. and Eyre, J. R.: Retrieving temperature, water vapour and surface pressure information from refractive-index profiles derived by radio occultation: a simulation study, Q. J. Roy. Meteorol. Soc., 126, 1661–1683, doi:10.1002/qj.49712656606, 2000. 4697

Highwood, E. J. and Hoskins, B. J.: The tropical tropopause, Q. J. Roy. Meteorol. Soc., 124, 1579–1604, doi:10.1002/qj.49712454911, 1998. 4695, 4702, 4708

Hoinka, K. P.: Statistics of the global tropopause pressure, B. Am. Meteorol. Soc., 126, 3303–3325, doi:10.1175/1520-0493(1998)126<3303:SOTGTP>2.0.CO;2, 1998. 4695

Holton, J. R., Haynes, P. H., McIntyre, M. E., Douglass, A. R., Rood, R. B., and Pfister, L.: Stratosphere–troposphere exchange, Rev. Geophys., 33, 403–439, doi:10.1029/95RG02097, 1995. 4695

Homeyer, C. R., Bowman, K. P., and Pan, L. L.: Extratropical tropopause transition layer characteristics from high-resolution sounding data, J. Geophys. Res., 115, D13108, doi:10.1029/2009JD013664, 2010. 4698

Kishore, P., Namboothiri, S. P., Igarashi, K., Jiang, J. H., Ao, C. O., and Romans, L. J.: Climatological characteristics of the tropopause parameters derived from GPS/CHAMP and GPS/SAC-C measurements, J. Geophys. Res., 111, D20110, doi:10.1029/2005JD006827, 2006. 4696

Kuo, Y.-H., Wee, T.-K., Sokolovskiy, S., Rocken, C., Schreiner, W., Hunt, D., and Anthes, R. A.: Inversion and error estimation of GPS radio occultation data, J. Meteorol. Soc. Jpn., 82, 507–531, 2004. 4696

Kursinski, E. R., Hajj, G. A., Schofield, J. T., Linfield, R. P., and Hardy, K. R.: Observing Earth's atmosphere with radio occultation measurements using the Global Positioning System, J. Geophys. Res., 102, 23429–23465, 1997. 4696, 4697

Kuttippurath, J. and Nikulin, G.: A comparative study of the major sudden stratospheric warmings in the Arctic winters 2003/2004–2009/2010, Atmos. Chem. Phys., 12, 8115–8129, doi:10.5194/acp-12-8115-2012, 2012. 4707

Lau, K.-M., Ho, C.-H., and Kang, I.-S.: Anomalous atmospheric hydrologic processes associated with ENSO: mechanisms of hydrologic cycle–radiation interaction, J. Climate, 11, 800–815, doi:10.1175/1520-0442(1998)011<0800:AAHPAW>2.0.CO;2, 1998. 4705

Leroy, S. S., Dykema, J. A., and Anderson, J. G.: Climate benchmarking using GNSS occultation, in: Atmosphere and Climate: Studies by Occultation Methods, edited by: Foelsche, U., Kirchengast, G., and Steiner, A. K., Springer, 287–302, 2006. 4696

AMTD
7, 4693–4727, 2014

Lewis, H. W.: A robust method for tropopause altitude identification using GPS radio occultation data, Geophys. Res. Lett., 36, L12808, doi:10.1029/2009GL039231, 2009. 4696
Melbourne, W. G., Davis, E. S., Duncan, C. B., Hajj, G. A., Hardy, K. R., Kursinski, E. R., Meehan, T. K., Young, L. E., and Yunck, T. P.: The Application of Spaceborne GPS to Atmospheric Limb Sounding and Global Change Monitoring, JPL Publication, 94–18, 147, 1994. 4696
NOAA: Stratosphere: Winter Bulletins, available at: http://www.cpc.ncep.noaa.gov/products/stratosphere/winter_bulletins/ (last access: 4 April 2014), NOAA/National Weather Service, NOAA Center for Weather and Climate Prediction, Climate Prediction Center, 2010. 4707
Randel, W. J., Wu, F., and Gaffen, D. J.: Interannual variability of the tropical tropopause derived from radiosonde data and NCEP reanalyses, J. Geophys. Res., 105, 15509–15523, doi:10.1029/2000JD900155, 2000. 4695, 4706
Randel, W. J., Seidel, D. J., and Pan, L. L.: Observational characteristics of double tropopauses, J. Geophys. Res., 112, D07309, doi:10.1029/2006JD007904, 2007. 4701
Santer, B. D., Sausen, R., Wigley, T. M. L., Boyle, J. S., AchutaRao, K., Doutriaux, C., Hansen, J. E., Meehl, G. A., Roeckner, E., Ruedy, R., Schmidt, G., and Taylor, K. E.: Behavior of tropopause height and atmospheric temperature in models, reanalyses, and observations: decadal changes, J. Geophys. Res., 108, D14002, doi:10.1029/2002JD002258, 2003. 4695
Santer, B. D., Wigley, T. M. L., Simmons, A. J., Kallberg, P. W., Kelly, G. A., Uppala, S. M., Ammann, C., Boyle, J. S., Brüggemann, W., Doutriaux, C., Fiorino, M., Mears, C. A., Meehl, G. A., Sausen, R., Taylor, K. E., Washington, W. M., Wehner, M. F., and Wentz, F. J.: Identification of anthropogenic climate change using a second-generation reanalysis, J. Geophys. Res., 109, D21104, doi:10.1029/2004JD005075, 2004. 4695
Sausen, R. and Santer, B. D.: Use of changes in tropopause height to detect human influences on climate, Meteorol. Z., 12, 131–136, doi:10.1127/0941-2948/2003/0012-0131, 2003. 4695
Scherllin-Pirscher, B., Kirchengast, G., Steiner, A. K., Kuo, Y.-H., and Foelsche, U.: Quantifying uncertainty in climatological fields from GPS radio occultation: an empirical-analytical error model, Atmos. Meas. Tech., 4, 2019–2034, doi:10.5194/amt-4-2019-2011, 2011. 4699
Scherllin-Pirscher, B., Deser, C., Ho, S.-P., Chou, C., Randel, W., and Kuo, Y.-H.: The vertical and spatial structure of ENSO in the upper troposphere and lower stratosphere from GPS radio occultation measurements, Geophys. Res. Lett., 39, L20801, doi:10.1029/2012GL053071, 2012. 4705

AMTD
7, 4693–4727, 2014

Schmidt, T., Wickert, J., Beyerle, G., and Reigber, C.: Tropical tropopause parameters derived from GPS radio occultation measurements with CHAMP, J. Geophys. Res., 109, D13105, doi:10.1029/2004JD004566, 2004. 4696

Schmidt, T., Heise, S., Wickert, J., Beyerle, G., and Reigber, C.: GPS radio occultation with CHAMP and SAC-C: global monitoring of thermal tropopause parameters, Atmos. Chem. Phys., 5, 1473–1488, doi:10.5194/acp-5-1473-2005, 2005. 4696

Schmidt, T., Wickert, J., Beyerle, G., and Heise, S.: Global tropopause height trends estimated from GPS radio occultation data, Geophys. Res. Lett., 35, L11806, doi:10.1029/2008GL034012, 2008. 4696

Schmidt, T., Wickert, J., and Haser, A.: Variability of the upper troposphere and lower stratosphere observed with GPS radio occultation bending angles and temperatures, Adv. Space Res., 46, 150–161, doi:10.1016/j.asr.2010.01.021, 2010. 4696

Schwärz, M., Scherllin-Pirscher, B., Kirchengast, G., Schwarz, J., Ladstädter, F., Fritzer, J., and Ramsauer, J.: Multi-Mission Validation by Satellite Radio Occultation, Wegener Center/Uni Graz final report for ESA/ESRIN No. 01/2013, Wegener Center for Climate and Global Change, University of Graz, 2013. 4698

Seidel, D. J. and Randel, W. J.: Variability and trends in the global tropopause estimated from radiosonde data, J. Geophys. Res., 111, D21101, doi:10.1029/2006JD007363, 2006. 4695

Seidel, D. J. and Randel, W. J.: Recent widening of the tropical belt: evidence from tropopause observations, J. Geophys. Res., 112, D20113, doi:10.1029/2007JD008861, 2007. 4695

Seidel, D. J., Ross, R. J., Angell, J. K., and Reid, G. C.: Climatological characteristics of the tropical tropopause as revealed by radiosondes, J. Geophys. Res., 106, 7857–7878, doi:10.1029/2000JD900837, 2001. 4695

Smith, E. and Weintraub, S.: The constants in the equation for atmospheric refractive index at radio frequencies, P. IRE, 41, 1035–1037, 1953. 4697

Son, S.-W., Tandon, N. F., and Polvani, L. M.: The fine-scale structure of the global tropopause derived from COSMIC GPS radio occultation measurements, J. Geophys. Res., 116, D20113, doi:10.1029/2011JD016030, 2011. 4696

Steiner, A. K., Lackner, B. C., Ladstädter, F., Scherllin-Pirscher, B., Foelsche, U., and Kirchengast, G.: GPS radio occultation for climate monitoring and change detection, Radio Sci., 46, RS0D24, doi:10.1029/2010RS004614, 2011. 4696

WMO: Meteorology – a three dimensional science, WMO Bull. 6, World Meteorological Organization (WMO), 1957. 4698

AMTD
7, 4693–4727, 2014

Yulaeva, E., Holton, J. R., and Wallace, J. M.: On the cause of the annual cycle in tropical lower-stratospheric temperatures, J. Atmos. Sci., 51, 169–174, doi:10.1175/1520-0469(1994)051<0169:OTCOTA>2.0.CO;2, 1994. 4703

Zängl, G. and Hoinka, K. P.: The tropopause in the polar regions, J. Climate, 14, 3117–3139, doi:10.1175/1520-0442(2001)014<3117:TTITPR>2.0.CO;2, 2001. 4700, 4702, 4703, 4704, 4708

AMTD

7, 4693–4727, 2014

Table 1. H_{mean} and H_{med} (km) in January and July 2008 for different latitudinal bands for first and second tropopause.

	First Tropopause				Second Tropopause			
	Jan 2008		Jul 2008		Jan 2008		Jul 2008	
	H_{mean}	H_{med}	H_{mean}	H_{med}	H_{mean}	H_{med}	H_{mean}	H_{med}
80–90° N	8.68	8.58	9.52	9.58	16.57	16.67	14.82	14.07
70–80° N	8.95	8.82	9.85	9.90	17.17	17.04	15.42	15.34
60–70° N	8.97	8.96	10.37	10.42	16.94	16.86	14.25	14.42
50–60° N	9.13	9.16	10.97	11.02	16.77	16.70	15.14	15.18
40–50° N	9.66	9.70	12.66	12.24	16.27	16.10	15.78	15.84
30–40° N	11.14	10.84	15.44	15.62	16.17	16.16	16.22	16.10
20–30° N	14.86	16.24	15.95	16.02	16.95	16.98	16.69	16.50
10–20° N	16.83	17.08	15.96	16.00	17.60	17.54	17.98	17.29
0–10° N	17.01	17.10	15.95	15.94	18.36	18.21	18.77	18.50
10–0° S	17.00	17.10	15.96	15.98	18.58	18.42	18.52	18.14
20–10° S	16.67	16.90	16.13	16.16	17.82	17.72	17.56	17.21
30–20° S	16.35	16.66	15.09	15.88	17.33	17.32	16.29	16.30
40–30° S	14.64	15.20	11.22	10.70	16.50	16.58	15.94	15.88
50–40° S	11.44	11.28	10.06	10.16	15.57	15.66	17.05	16.74
60–50° S	9.41	9.30	9.90	10.02	14.72	14.74	17.59	17.76
70–60° S	8.68	8.64	10.20	10.04	15.04	15.17	16.27	16.08
80–70° S	8.48	8.42	11.06	10.36	14.55	14.78	15.79	15.76
90–80° S	8.18	8.08	11.59	10.46	16.52	15.76	15.83	16.04

AMTD
7, 4693–4727, 2014

Table 2. T_{mean} and T_{med} (K) in January and July 2008 for different latitudinal bands for first and second tropopause.

	First Tropopause				Second Tropopause			
	Jan 2008		Jul 2008		Jan 2008		Jul 2008	
	T_{mean}	T_{med}	T_{mean}	T_{med}	T_{mean}	T_{med}	T_{mean}	T_{med}
80–90° N	210	210	222	221	198	197	228	229
70–80° N	209	209	221	221	198	198	226	227
60–70° N	212	212	220	220	205	203	224	225
50–60° N	214	214	220	219	214	214	220	220
40–50° N	216	215	216	216	215	215	215	215
30–40° N	216	216	205	204	209	209	208	208
20–30° N	204	200	199	198	202	201	204	205
10–20° N	193	192	196	195	197	197	201	201
0–10° N	189	189	195	195	193	193	202	201
10–0° S	189	189	195	195	194	194	201	200
20–10° S	192	191	196	196	198	198	198	197
30–20° S	197	196	204	201	200	200	205	204
40–30° S	208	206	217	216	206	206	211	211
50–40° S	217	217	214	214	213	213	213	213
60–50° S	221	221	211	210	220	220	207	206
70–60° S	220	220	206	206	226	226	198	197
80–70° S	219	218	199	200	225	225	191	190
90–80° S	219	219	196	196	231	230	187	186

AMTD
7, 4693–4727, 2014

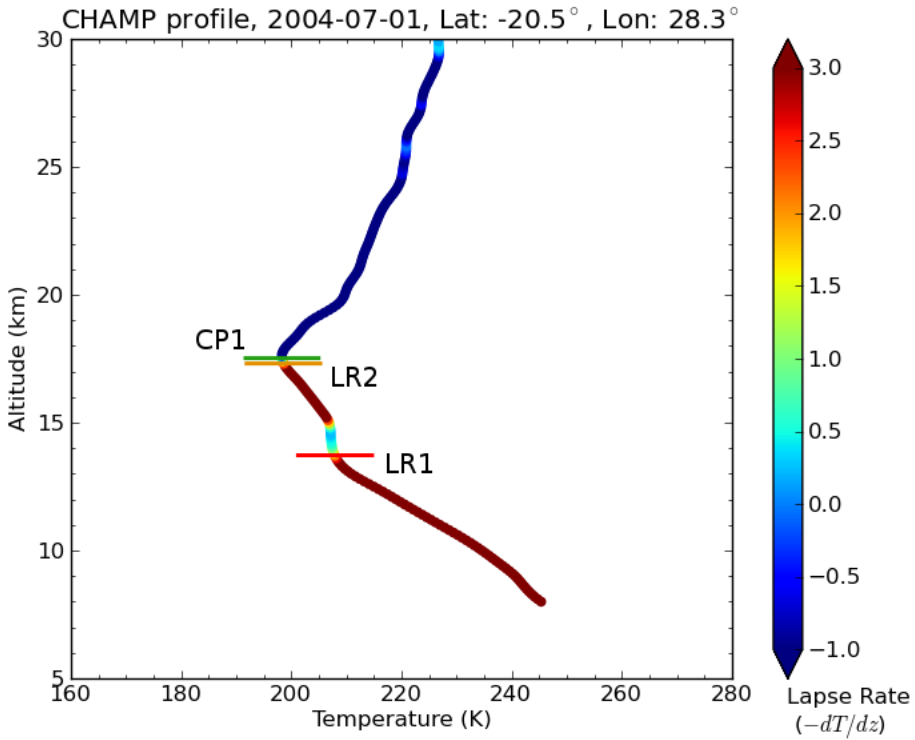

Fig. 1. CHAMP temperature profile colored according to its lapse rate. Horizontal bars indicate the lowest (first) lapse rate tropopause (LR1), second lapse rate tropopause (LR2), and the local minimum of the profile, the cold point tropopause (CP1). Note the decrease in temperature above LR1, fulfilling the requirement for a second tropopause (lapse rate greater than 3 °C km^{-1}).

AMTD
7, 4693–4727, 2014

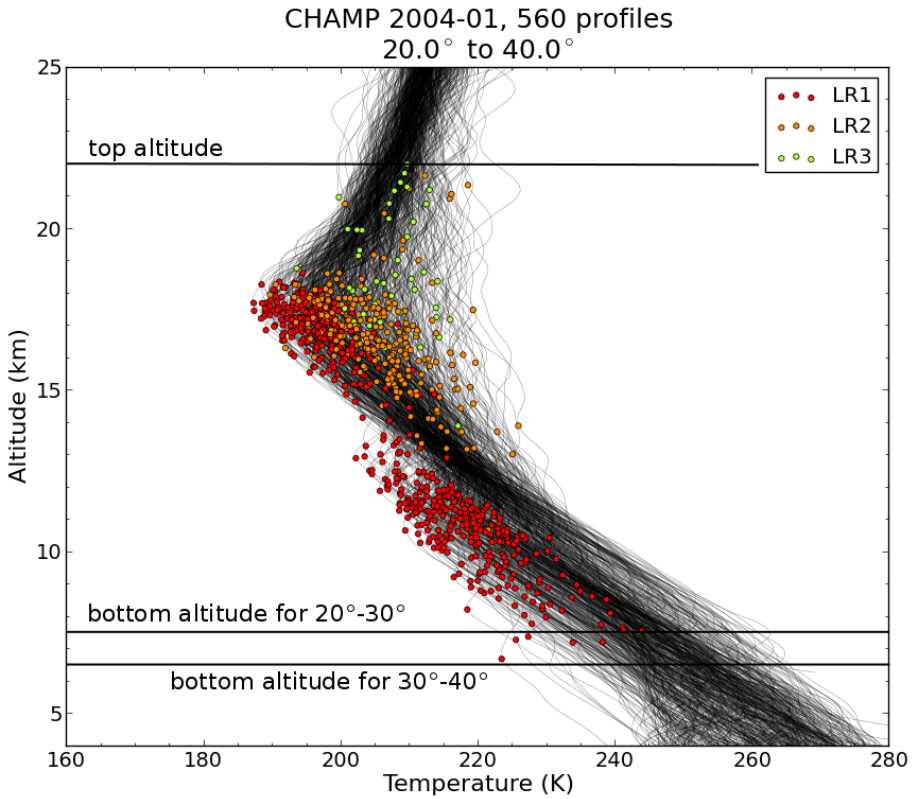

Fig. 2. CHAMP temperature profiles and their tropopauses between 20° N and 40° N in January 2004. First tropopause: red, second tropopause: orange, third tropopause: green. Top and bottom altitudes of the tropopause algorithm are indicated by horizontal lines.

AMTD
7, 4693–4727, 2014

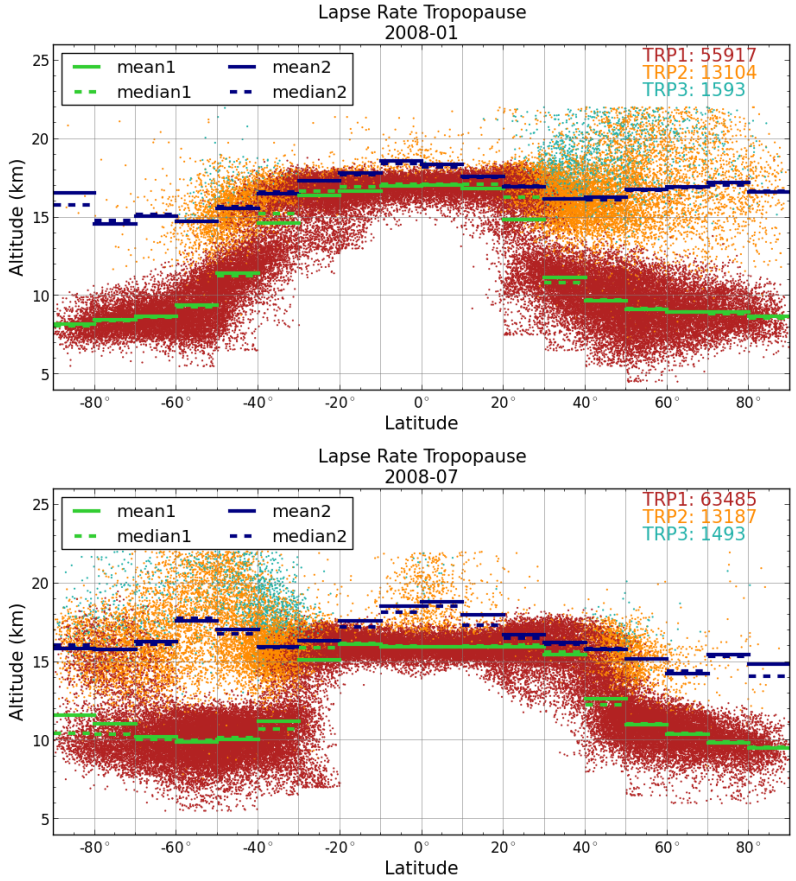

Fig. 3. Altitudes of the first (lowest, red), second (orange), and third (blue) tropopause vs. latitude for January (top) and July (bottom) 2008. Mean (solid) and median (dashed) of first (green) and second (blue) tropopause of 10° latitudinal bands are indicated by horizontal lines.

AMTD
7, 4693–4727, 2014

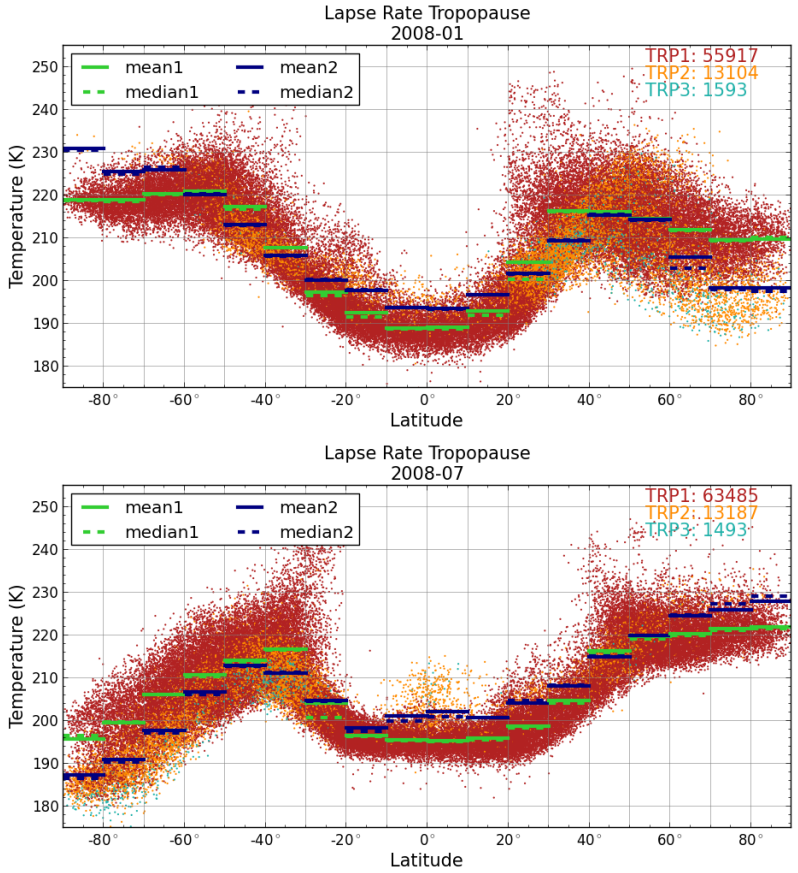

Fig. 4. Temperatures of the first (lowest, red), second (orange), and third (blue) tropopause vs. latitude for January (top) and July (bottom) 2008. Mean (solid) and median (dashed) of first (green) and second (blue) tropopause of 10° latitudinal bands are indicated by horizontal lines.

AMTD
7, 4693–4727, 2014

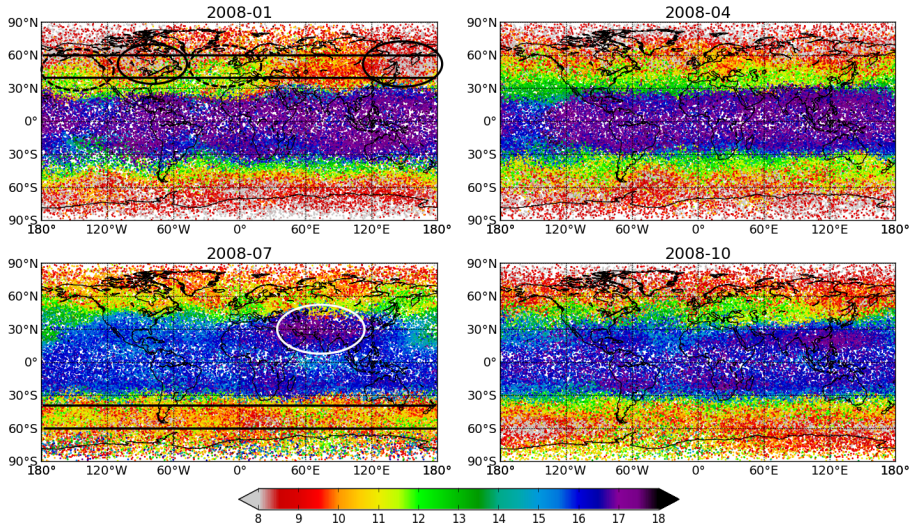

Fig. 5. Altitude of first tropopauses for January, April, July, and October 2008 (given in km).

AMTD
7, 4693–4727, 2014

Characteristics of tropopause parameters

T. Rieckh et al.

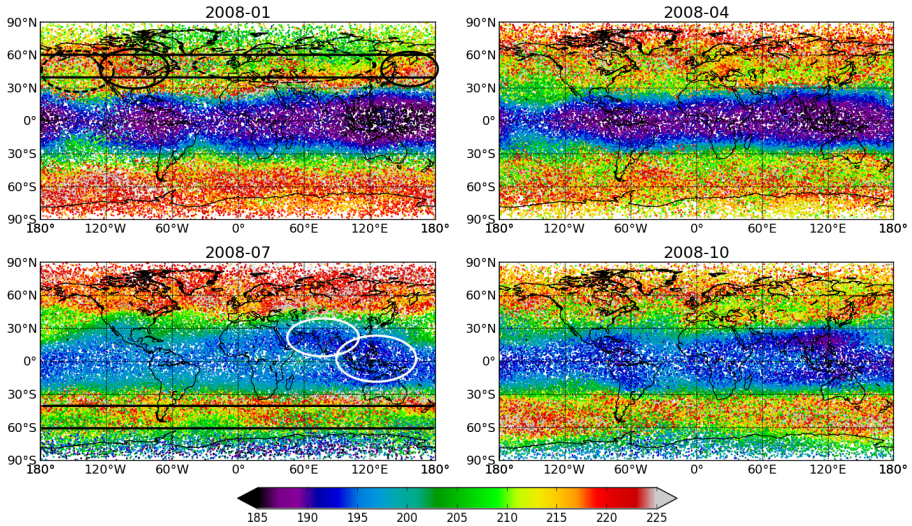

Fig. 6. Temperature of first tropopauses for January, April, July, and October 2008 (given in K).

AMTD
7, 4693–4727, 2014

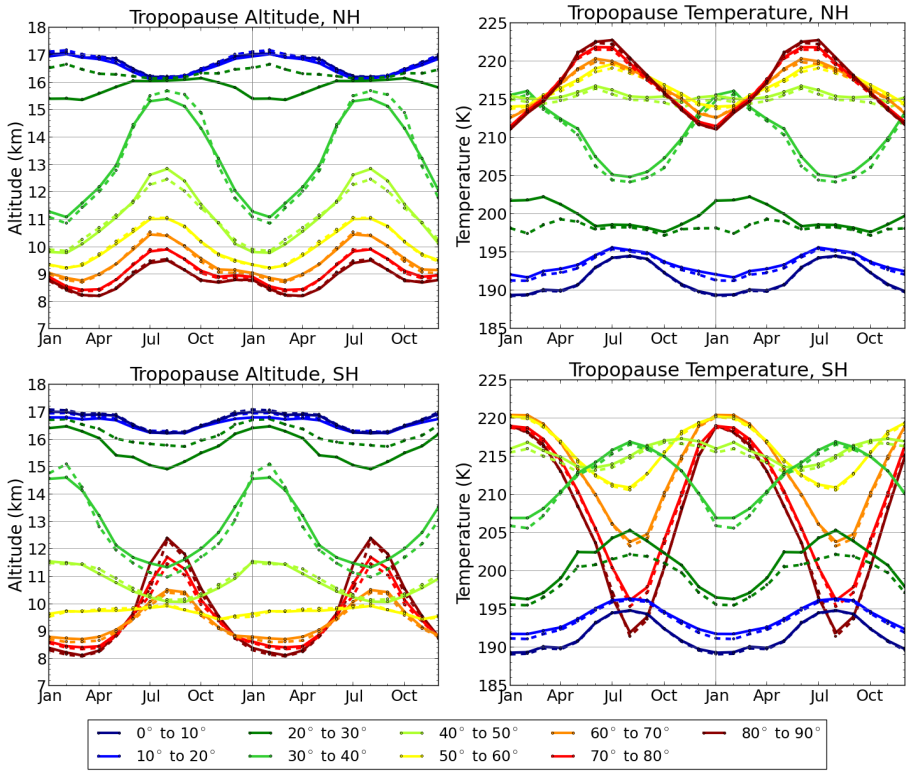

Fig. 7. Annual cycle of mean (solid) and median (dashed) for tropopause altitude (left) and temperature (right) (top: NH, bottom: SH). Colors indicate different latitudinal bands. To give a better overview, two full cycles are shown.

AMTD
7, 4693–4727, 2014

Characteristics of tropopause parameters

T. Rieckh et al.

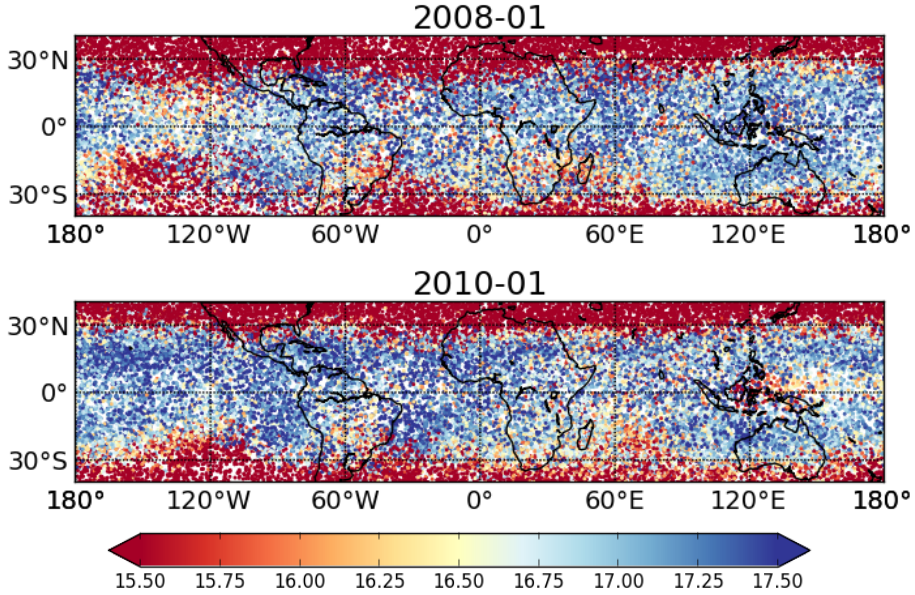

Fig. 8. The effect of ENSO cold (top) and warm (bottom) phases: tropopause altitude (km).

AMTD
7, 4693–4727, 2014

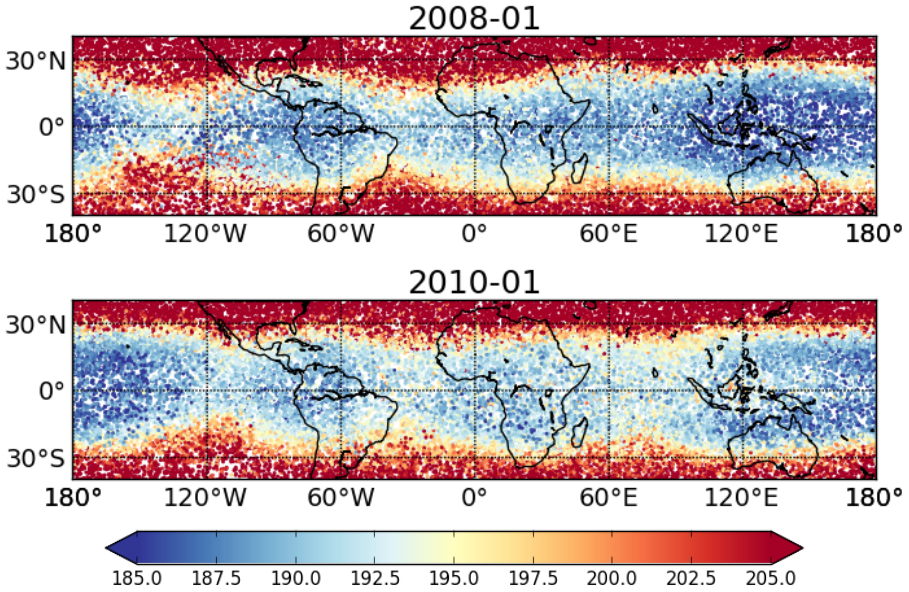

Fig. 9. The effect of ENSO cold (top) and warm (bottom) phases: tropopause temperature (K).

AMTD
7, 4693–4727, 2014

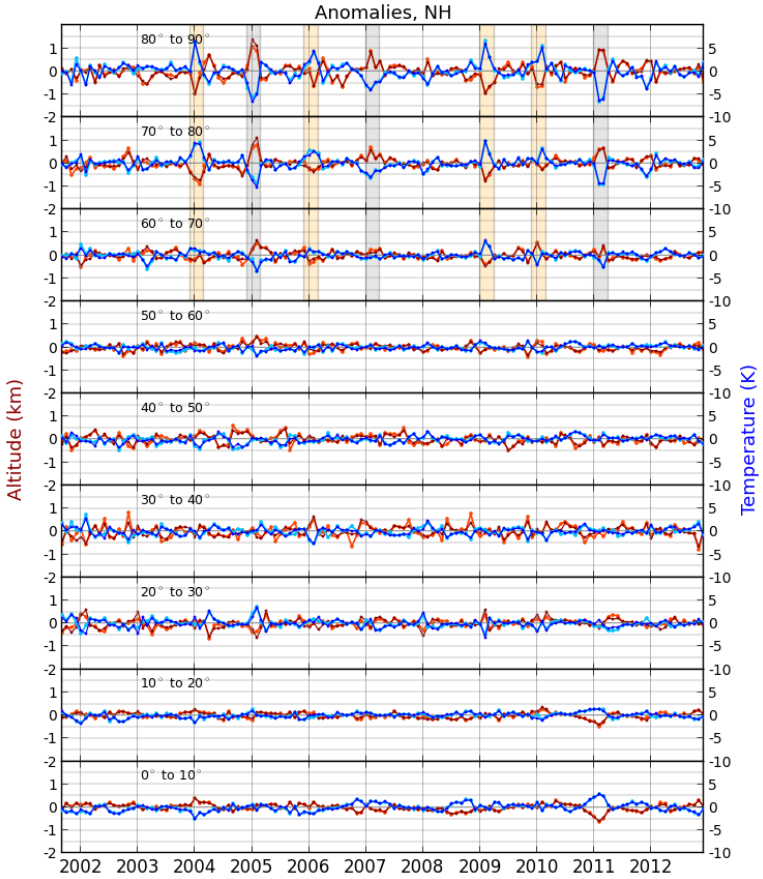

Fig. 10. Anomalies of H_T (mean: red, median: orange) and T_T (mean: dark blue, median: light blue) for 10° latitudinal bands in the NH, time range: September 2001 to December 2012. Months with strong SSW events are highlighted in orange, months with very weak or no events are highlighted in gray.

AMTD
7, 4693–4727, 2014

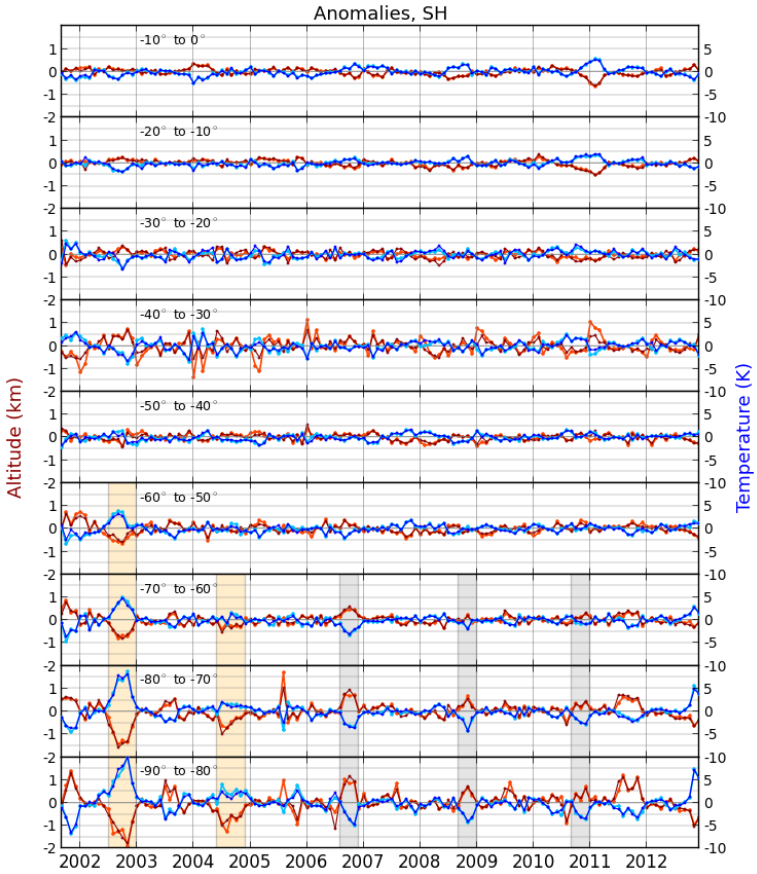

Fig. 11. Anomalies of H_T (mean: red, median: orange) and T_T (mean: dark blue, median: light blue) for 10° latitudinal bands in the SH, time range: September 2001 to December 2012. Months with exceptionally warm/cool stratospheric conditions are highlighted in orange and gray, respectively.

AMTD
7, 4693–4727, 2014